Plant Physiology Preview. Published on May 19, 2020, as DOI:10.1104/pp.20.00090

Running title: Retrograde coordinates light and hormone signals

Corresponding Author:

Katayoon Dehesh

Department of Botany and Plant Sciences, Institute of Integrative Genome Biology, University of California Riverside, CA, 92521, USA.

Tel: 951-827-6370

E-Mail: kdehesh@ucr.edu

Retrograde induction of phyB orchestrates ethylene-auxin hierarchy to regulate growth

Jishan Jiang[1+], Yanmei Xiao[2], Hao Chen[1],Wei Hu[2] , Liping Zeng[1], Haiyan Ke[1], Franck A.Ditengou[4], Upendra Devisetty[3,5], Klaus Palme[4], Julin Maloof [3], Katayoon Dehesh[1*]

Affiliations

[1]Department of Botany and Plant Sciences, Institute of Integrative Genome Biology, University of California, Riverside, CA, 92521, USA.

[2]Department of Molecular and Cellular Biology, University of California, Davis, CA 95616, USA.

[3]Department of Plant Biology, University of California, Davis, CA, 95616, USA.

[4] University of Freiburg, Faculty of Biology; BIOSS Centre for Biological Signaling Studies and ZBSA Centre for Biosystems Studies, Schänzler str.1, 79104 Freiburg, Germany.

[5]Current address: Thomas W. Keating Bioresearch Building, University of Arizona, Tucson, Arizona, 85721, USA.

+ Current address: College of Grassland Science and Technology, China Agricultural University, Beijing, China.

*To whom correspondence should be addressed

One-sentence summary: The plastidial retrograde metabolite MEcPP orchestrates coordination of light and hormonal signaling cascade by inducing phytochrome B abundance and modulating auxin and ethylene levels.

Author Contributions

J.J. and K.D. designed the study, J.J., Y.X., H.C. W.H., U.D., H.K., and F.D. performed the experiments, L.Z performed the bioinformatics analyses, J.M. and K.P. provided experimental tools and K.D. wrote the manuscript.

Financial source: This work was supported by National Institute of Health (R01GM107311) grant awarded to KD.

The author responsible for distribution of materials integral to the findings presented in this article is Katayoon Dehesh (kdehesh@ucr.edu).

Abstract

Exquisitely regulated plastid-to-nucleus communication by retrograde signaling pathways is essential for fine-tuning of responses to the prevailing environmental conditions. The plastidial retrograde signaling metabolite methylerythritol cyclodiphosphate (MEcPP) has emerged as a stress signal transduced into a diverse ensemble of response outputs. Here we demonstrate enhanced phytochrome B protein abundance in red light–grown MEcPP-accumulating *ceh1* mutant plants relative to wild-type seedlings. We further establish MEcPP-mediated coordination of phytochrome B with auxin and ethylene signaling pathways and uncover differential hypocotyl growth of red light–grown seedlings in response to these phytohormones. Genetic and pharmacological interference with ethylene and auxin pathways outline the hierarchy of responses, placing ethylene epistatic to the auxin signaling pathway. Collectively, our findings establish a key role of a plastidial retrograde metabolite in orchestrating the transduction of a repertoire of signaling cascades. This work positions plastids at the zenith of relaying information coordinating external signals and internal regulatory circuitry to secure organismal integrity.

Introduction

Dynamic alignment of internal and external cues through activation of corresponding signal transduction pathways is a defining characteristic of organisms essential for fitness and the balancing act of metabolic investment in growth versus adaptive responses. The integrity of these responses is achieved through finely controlled communication circuitry, notably retrograde (organelle-to-nucleus) signaling cascades. Despite the central role of retrograde signaling in regulation and coordination of numerous adaptive processes, the nature and the operational mode of action of retrograde signals have remained poorly understood.

Through a forward-genetic screen, we identified a bifunctional plastid-produced metabolite methylerythritol cyclodiphosphate (MEcPP) that serves as a precursor of isoprenoids produced by the plastidial methylerythritol phosphate (MEP) pathway and functions as a stress-specific retrograde signaling metabolite (Xiao et al., 2012). We further demonstrated that stress-induced MEcPP accumulation leads to growth retardation and induction of selected nuclear-encoded, stress-response genes (Xiao et al., 2012; Walley et al., 2015; Lemos et al., 2016; Wang et al., 2017a). We specifically established that regulation of growth is in part via MEcPP-mediated modulation of levels and distribution patterns of auxin (IAA) through dual transcriptional and post-translational regulatory inputs (Jiang et al., 2018).

Auxin functions as a key hormone regulating a repertoire of plant development processes including hypocotyl growth (J. Jensen et al., 1998; De Grauwe et al., 2005). The auxin biosynthesis pathway that converts tryptophan (Trp) to IAA in plants is established to be through conversion of Trp to indole-3-pyruvate (IPA) by the TAA family of amino transferases and subsequent production of IAA from IPA by the YUC family, a family of flavin monooxygenases (Zhao, 2012). Subsequently, establishment of auxin gradient is achieved by transporters such as the auxin-efflux carrier PIN-FORMED1 (PIN1) (Galweiler et al., 1998; Geldner et al., 2001). Interestingly, IAA biosynthesis, transport, and signaling during light–mediated hypocotyl growth

are in turn regulated by ethylene (Liang et al., 2012), and conversely ethylene is regulated by auxin (Vandenbussche et al., 2003; Ruzicka et al., 2007; Stepanova et al., 2007; Swarup et al., 2007; Negi et al., 2010). As such, auxin-ethylene crosstalk inserts an additional layer of complexity to the already intricate and multifaceted growth regulatory mechanisms.

Ethylene in plants is derived from conversion of S-adenosyl-L-methionine (AdoMet) to 1-aminocyclopropane-1-carboxylate (ACC) by ACC synthase (ACS) (Yang and Hoffman, 1984), followed by conversion of ACC to ethylene catalyzed by ACC oxidase (L.-C. Wang et al., 2002). Ethylene stimulates hypocotyl growth in the light but inhibits it in the dark (Smalle et al., 1997; J. Jensen et al., 1998; Vandenbussche et al., 2012).

Light signaling is a common environmental stimulus controlling developmental processes through hormonal modulation, such as regulation of auxin biosynthesis and signaling genes by phytochrome B (phyB) (Morelli and Ruberti, 2002; Tanaka et al., 2002b; Tian et al., 2002; Nozue et al., 2011; Hornitschek et al., 2012a; de Wit et al., 2014; Leivar and Monte, 2014). PhyB is the main photoreceptor mediating red-light photomorphogenesis; phyB is activated by red light and imported into the nucleus where it forms phyB-containing nuclear bodies (phyB-NBs) (Nagy and Schafer, 2002; Quail, 2002). Formation of phyB-NBs depends on binding to and sequestration of the basic helix-loop-helix (bHLH) transcription factors, Phytochrome Interacting Factor 1 (PIF1), PIF3, PIF4, PIF5, and PIF7 (Rausenberger et al., 2010; Leivar and Quail, 2011). The prominent role of phyB in auxin regulation is best displayed by simulation of shade avoidance responses (SAR) through exogenous application of auxin or via genetic manipulation of auxin (Tanaka et al., 2002a; Hornitschek et al., 2012b). In addition, PIFs, specifically PIF4, PIF5, and PIF7, play a major role in regulating auxin by targeting promoter elements of multiple auxin biosynthetic and signal transduction genes (Franklin et al., 2011; Nozue et al., 2011; Leivar et al., 2012; Sellaro et al., 2012; Leivar and Monte, 2014). Moreover, the ethylene–promoted hypocotyl elongation in light is regulated by the PIF3-dependent, growth-promoting pathway

activated transcriptionally by EIN3, whereas under dark conditions, ethylene inhibits growth by destabilizing the ethylene response factor 1 (ERF1) (Zhong et al., 2012). Here, we identify MEcPP as a retrograde signaling metabolite that coordinates internal and external cues, and we further delineate light and hormonal signaling cascades that elicit adaptive responses to ultimately drive growth-regulating processes tailored to the prevailing environment.

Results

Elevated phyB abundance suppresses hypocotyl growth in ceh1

Given the stunted hypocotyl phenotype of the high MEcPP–accumulating mutant *ceh1*, we explored the nature of the photoreceptors involved by examining hypocotyl length of seedlings grown in the dark and under various monochromatic light conditions. The analyses showed comparable hypocotyl lengths of dark-grown *ceh1* and control seedlings (WT) (Fig. 1**A**). However, under continuous red light (Rc; 15 μE $m^{-2}sec^{-1}$), *ceh1* seedlings displayed notably shorter hypocotyls than those of WT plants (Fig. 1**A**). This data led us to question the role of phyB, the prominent red-light photoreceptor, in regulating *ceh1* hypocotyl growth. To answer this question, we generated a *ceh1/phyB-9* double-mutant line, and subsequently compared seedling hypocotyl length with WT, *ceh1*, and *phyB-9* seedlings grown under continuous dark and Rc conditions (Fig. 1**A** & **B**). The data clearly demonstrated phyB-dependent suppression of hypocotyl growth in *ceh1* under Rc, as evidenced by the recovery of *ceh1* retarded hypocotyl growth in *ceh1/phyB-9* to lengths comparable to those of *phyB-9* seedlings.

Hypocotyl growth of the aforementioned four genotypes was also examined under continuous blue (Bc) and far-red (FRc) light conditions. The reduced hypocotyl growth of the *ceh1* mutant grown under Bc, albeit not as severe as those grown under Rc, further implicate blue light–receptor cytochromes (Yu et al., 2010) in regulating growth of these seedlings (Fig. S1**A** & **B**). Additionally, *ceh1* and *ceh1/phyB-9* seedlings grown under Bc exhibited equally shortened hypocotyls, and under FRc light hypocotyl growth was almost similarly retarded in all genotypes (Fig. S1**A** & **B**). Collectively, these results support the involvement of cryptochromes as well as phyB in *ceh1* hypocotyl growth, albeit to different degrees. However, the more drastic effect of phyB in regulating hypocotyl growth of Rc-grown, high MEcPP–accumulating seedlings, in conjunction with the supporting evidence from earlier data using white light–grown *ceh1* seedlings (Jiang et al., 2019), led us to primarily focus on the role of phyB.

Next, we measured MEcPP levels in the four genotypes grown in the dark and in

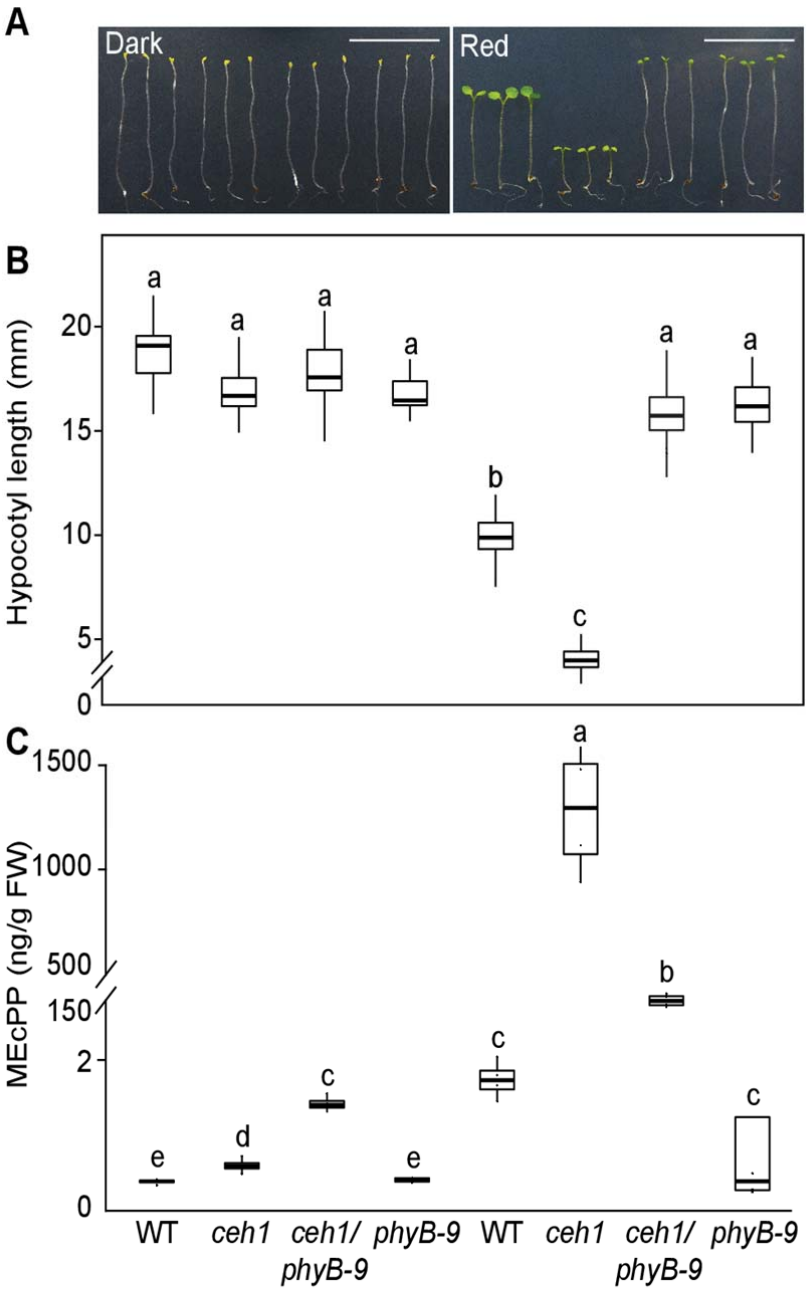

Fig. 1. *Ceh1* hypocotyl growth in red light is phyB-dependent (**A**) Representative images of 7-day-old WT, *ceh1*, *ceh1*/*phyB-9* and *phyB-9* seedlings grown in the dark and continuous red light (Rc: 15 $\mu Em^{-2}sec^{-1}$). (**B**) Quantification of hypocotyl lengths from aforementioned genotypes shown in Fig.1**A**. (**C**) MEcPP levels of samples from Fig.1**A**. The break indicates a change of scale on the y axis. Statistical analyses were performed using Tukey's HSD method (n ≥), different letters indicate significant difference ($P < 0.05$). Scale bars: 1cm.

various monochromatic wavelengths to examine a potential correlation between

growth phenotypes and altered levels of the retrograde signaling metabolite (Fig. 1**C** & S1**C**). The analyses showed almost undetectable MEcPP levels in dark-grown plants of all the genotypes, and low levels of the metabolite in Rc-grown WT and *phyB-9* seedlings. By contrast, *ceh1* seedlings grown in Rc accumulated high MEcPP levels, a phenotype that was partially (~10-fold) suppressed in *ceh1/phyB-9* seedlings. This reduction was not unexpected since phyB-controlled PIF regulates the expression of *DXS*, the first MEP-pathway gene encoding the flux determinant enzyme (Chenge-Espinosa et al., 2018). It is noteworthy that despite this significant reduction, the MEcPP content of *ceh1/phyB-9* seedlings remained ~100-fold above those of WT or *phyB-9* plants grown simultaneously and under the same conditions. This reduction of MEcPP in *ceh1*/*phyB-9* also occurred in seedlings grown in Bc (Fig. S1**C**), likely because of the direct interaction between PIFs and blue light–receptor cryptochromes (Pedmale et al., 2016). However, in spite of reduced MEcPP levels in Rc- or Bc-grown *ceh1/phyB-9* seedlings, the hypocotyl growth recovery is exclusive to mutant seedlings grown in Rc (Fig. 1**A**-**C** & S1**A**-**C**), leading to the conclusion that there is also a blue light–dependent pathway that regulates *ceh1* hypocotyl growth in Bc. Moreover, hypocotyls of all genotypes, regardless of their MEcPP levels, remained stunted in FRc, a light condition known to inactivate phyB. Collectively, the results further verify the function of phyB in altering the observed growth phenotype of *ceh1* mutant seedlings.

To examine the correlation between accumulation of MEcPP and alteration of growth in response to red-light treatment, we further examined the hypocotyl length of Col-0 ecotype, Col-0 transformed with *HPL:LUC* construct (WT), *ceh1*, and complemented *ceh1* (CP) seedlings (Fig. 2**A**-**B**). In contrast to the stunted hypocotyl growth of *ceh1*, these data clearly showed recovery of hypocotyl growth in CP to lengths comparable to Col-0 and WT seedlings (Fig. 2**A**-**B**).

Next, we questioned whether phyB transcript and/or protein levels are altered in *ceh1* mutants grown in Rc. The expression data analyses revealed similar *PHYB* transcript levels in *ceh1* and WT seedlings (Fig. S1**D**). To determine the hyB protein levels, we performed immunoblot analyses using proteins isolated from the aforementioned

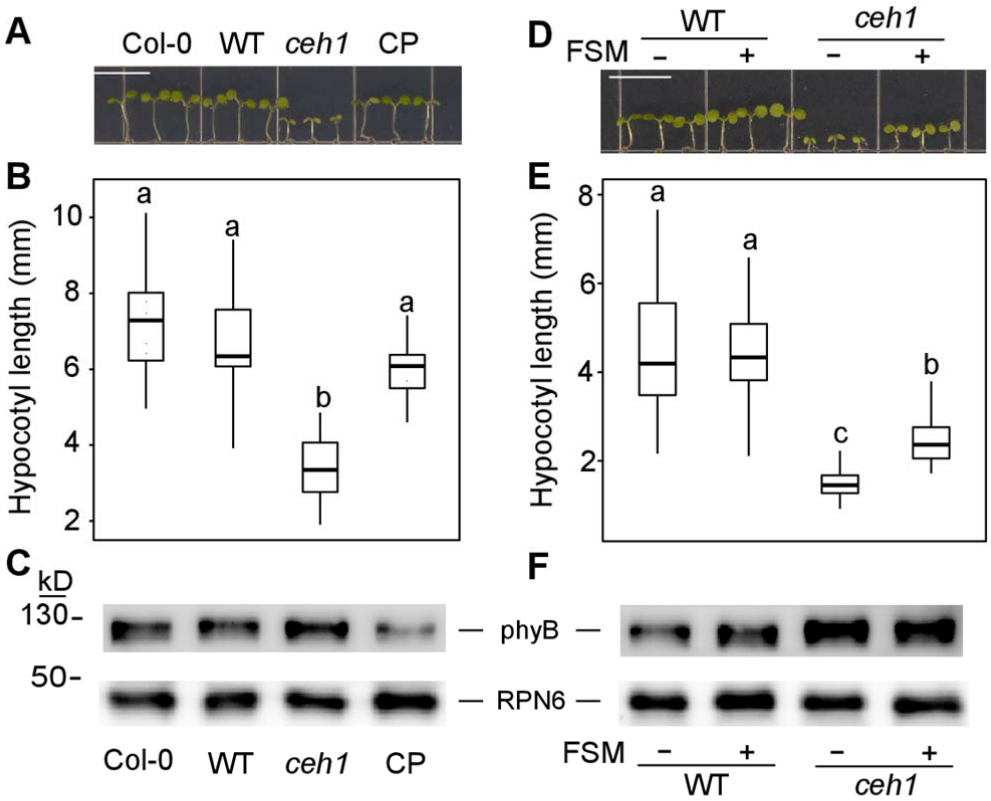

Fig. 2. MEcPP induction of phyB results in stunted *ceh1* hypocotyl growth
(**A**) Reprentative images of 7-day-old Col-0, WT, *ceh1* and complementation line (CP) seedlings grown in Rc15 (15 $\mu Em^{-2}sec^{-1}$). Scale bars: 1 cm.
(**B**) & (**E**) Quantification of hypocotyl length of seedlings from panel (**A**) and (**D**), respectively. Data are presented with 45 seedlings. Statistical analyses were carried out using Tukey's HSD method, different letters indicate significant difference ($P < 0.05$). (**C**) & (**F**) Immunoblots of phyB protein abundance, using RPN6 antibody a loading control.
(**D**) Representative images of 7-day-old WT and *ceh1* seedlings grown in Rc15 (15 $\mu Em^{-2}sec^{-1}$) in the absence (-) and presence (+) of fosmidomycin (20 μM).

genotypes (Fig. 2**C**). The data showed higher PhyB levels in *ceh1* versus other genotypes specifically as compared with the complemented line (CP), supporting conclusion that MEcPP mediates enhanced abundance of phyB.

To further examine the potential role of MEcPP in *ceh1* in reducing growth and altering phyB levels, we employed a pharmacological approach using fosmidomycin (FSM), a MEP-pathway inhibitor (Fig. 2**D**-**F**). This inhibitor interferes with and highly reduces the flux through the pathway and abolishes MEcPP-mediated actions such as formation of otherwise stress–induced subcellular structures known as ER

bodies or furthering the reduced auxin levels in *ceh1* mutant plants (Gonzalez-Cabanelas et al., 2015; Wang et al., 2017b; Jiang et al., 2018). We examined hypocotyl growth of red light–grown 7-day-old seedlings that were treated with FSM for 3 days. These data showed enhanced hypocotyl growth of FSM-treated *ceh1* compared to non-treated seedlings (Fig. 2**D**-**E**). It is of note that the length of FSM-treated *ceh1* hypocotyls did not recover to that of the WT seedlings, suggesting an inefficiency of FSM treatment and/or the presence of other regulatory factors. In addition, immunoblot analysis showed a very slight reduction in phyB abundance in FSM-treated *ceh1* compared to non-treated seedling (Fig. 2**F**). There may be two reasons for not detecting an overall stronger response to FSM treatment. One is the very high MEcPP levels in the *ceh1* mutant, and the other the degree of FSM penetration. However, the clearly higher PhyB levels in the *ceh1* mutant compared to CP, WT, and Col lines supports the notion of MEcPP-mediated increase of phyB abundance, verifying the earlier report using white light–grown seedlings (Jiang et al., 2019).

In addition to MEcPP, the *ceh1* mutant accumulates substantial amounts of the defense hormone salicylic acid (SA) (Xiao et al., 2012; Bjornson et al., 2017). The reported involvement of phyB in SA accumulation and signaling (Chai et al., 2015; Nozue et al., 2018) prompted us to examine the potential role of this defense hormone in regulating *ceh1* hypocotyl growth. For these experiments, we employed the previously generated SA-deficient double-mutant line *ceh1*/*eds16* (Xiao et al., 2012). All four genotypes (WT, *ceh1*, *ceh1/eds16*, and *eds16*) displayed similar hypocotyl length when grown in the dark, whereas in Rc both *ceh1* and *ceh1/eds16* seedlings displayed equally reduced hypocotyl lengths as compared to their respective control backgrounds (Fig. S1**G**). These results illustrate SA-independent regulation of *ceh1* hypocotyl growth in Rc.

Given the well-established role of PIFs in transduction of phyB signals, we examined *PIF*s expression levels and found significantly reduced *PIF4* and -*5* transcripts in Rc-grown *ceh1* compared to WT seedlings (Fig. S2). These data led us to genetically investigate the potential role of PIFs in regulating hypocotyl length of Rc-grown *ceh1*

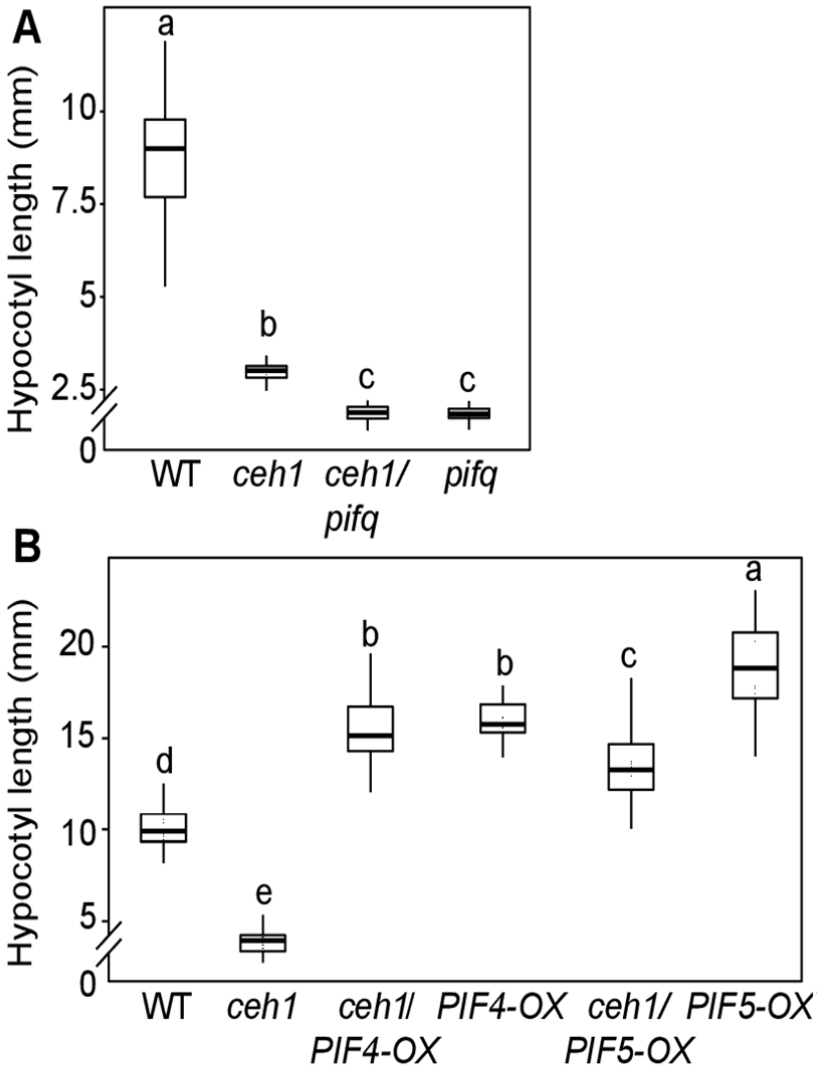

Fig. 3. Overexpression of *PIF4* and *PIF5* recover stunted hypocotyl growth of *ceh1*

(**A**) Quantification of hypocotyl lengths of 7-day-old WT, *ceh1*, *ceh1*/*pifq*, and *pifq* grown in Rc (15 $\mu Em^{-2}sec^{-1}$).

(**B**) Quantification of hypocotyl lengths from 7-day-old WT, *ceh1*, *ceh1*/*PIF4-OX*, *PIF4-OX*, *ceh1*/*PIF5-OX* and *PIF5-OX* grown in Rc (15 $\mu Em^{-2}sec^{-1}$). Data are presented with n≥20 for the *pif* mutant backgrounds and n≥30 for the experiments containing *PIF-OX* seedlings. The break indicates a change of scale on the y axis. Statistical analyses were carried out using Tukey's HSD method, different letters indicate significant difference.

253 seedlings. For these experiments, we quantified hypocotyl growth of *pifq (pif1*, *-3*, *-4*,

and *-5)* alone and in lines introgressed into the *ceh1* mutant background. The results revealed similarly dwarf hypocotyls in *ceh1*/*pifq* and *pifq* backgrounds, which were slightly but significantly shorter than that of *ceh1* seedlings (Fig. 3**A**). Furthermore, equally reduced hypocotyl growth in *ceh1*/*pifq* and *pifq* suggest that PIFs are the predominant growth regulators in *ceh1* under the experimental conditions employed. The role of PIFs in determining hypocotyl growth was further tested by examining *ceh1* seedlings overexpressing *PIF4* and *-5* grown in Rc (Fig. 3**B**). The data showed the expected enhanced hypocotyl growth of *PIF* overexpressors compared to WT seedlings and recovery of the retarded growth observed in *ceh1* in *ceh1*/*PIF4* and *-5* overexpression lines.

Collectively, these data illustrate growth regulatory function of PIFs, and identify MEcPP–mediated transcriptional regulation of *PIF4* and *-5* as an integral regulatory circuit controlling *ceh1* hypocotyl growth.

Reduced expression of auxin biosynthesis and response genes in ceh1

To identify the downstream components of the MEcPP–mediated phyB signaling cascade, we performed RNAseq profiling of WT and *ceh1* seedlings grown in the dark and in Rc. A multi-dimensional scaling (MDS) plot revealed significant overlap between expression profiles of WT and *ceh1* seedlings grown in the dark, in contrast to their distinct expression profiles when grown in Rc (Fig. S3). GO-term analyses identified over-representations of auxin signaling and response genes amongst the significantly (≥2-fold) altered transcripts (Fig. S4). Confirmation of the data through RT-qPCR identified auxin biosynthesis (*YUC3* and *-8*) and response genes (*IAA6* and *-19*) as the most significantly differentially expressed genes under Rc conditions (Fig. 4**A-B**). We further quantified the IAA content in plants and found similar auxin levels in dark-grown plans of all genotypes in contrast to significantly reduced auxin levels (50%) in Rc-grown *ceh1* versus WT plants (Fig. 4**C**). We validated this finding by testing Rc-grown WT and *ceh1* lines expressing the auxin signaling reporter *DR5*-GFP (Jiang et al., 2018). The reduced GFP signal in *ceh1* was on par with lower IAA levels in the mutant compared to the WT seedling (Fig. 4**D**).

Next, we examined possible modulation of other phytohormones such as abscisic acid

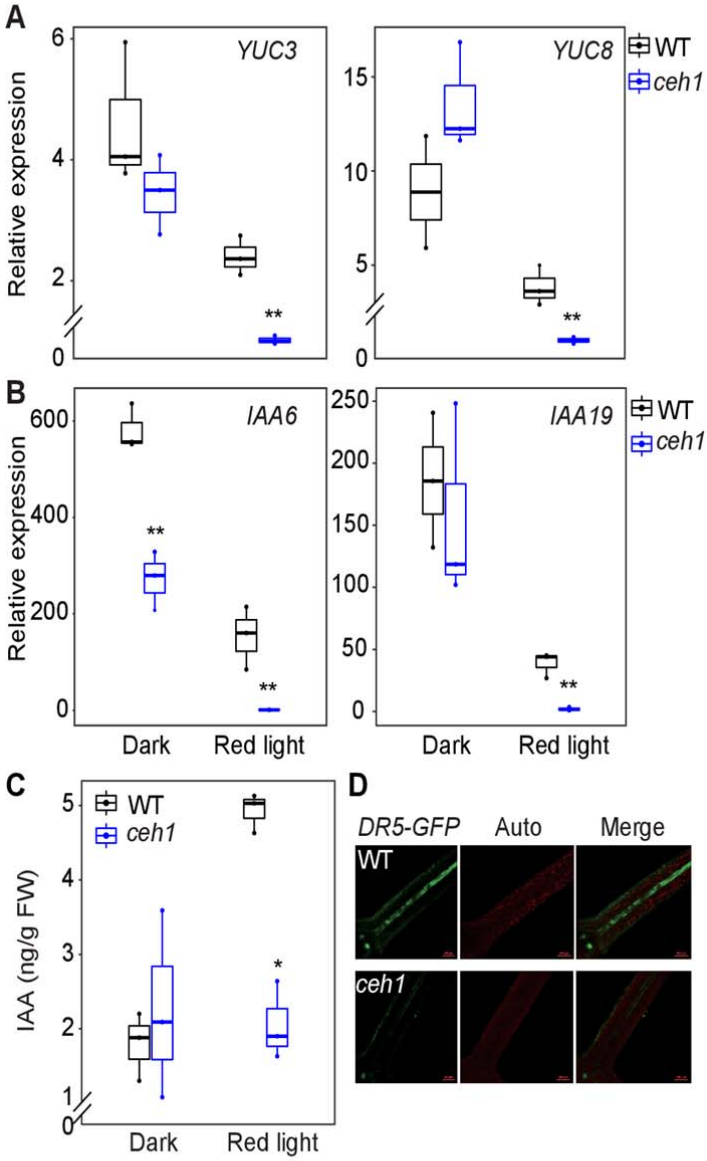

Fig. 4. Auxin is reduced in *ceh1*

Expression levels of *YUC3*, *8* (**A**) and *IAA6*, *19* (**B**) in WT and *ceh1* seedlings. RNAs were extracted from 7-day-old WT and *ceh1* seedlings grown in the dark and Rc (15 $\mu Em^{-2}sec^{-1}$). Transcript levels of target genes were normalized to the levels of At4g26410 (M3E9). Data are presented with three biological replicates and three technical replicates. Statistical analyses were determined by a two-tailed Student's *t* tests with a significance of $P < 0.05$ *, $P < 0.01$ **.

(**C**) IAA levels in 7-day-old WT and *ceh1* seedlings grown in the dark and Rc (15 $\mu Em^{-2}sec^{-1}$). Data are presented with three biological replicates. The break indicates a change of scale on the y axis. Statistical analyses were carried out by a two-tailed Student's *t* tests with a significance of $P < 0.05$. (**D**) Representative images of *DR5-GFP* signal intensity in 7-day hypocotyls of Rc (15 $\mu Em^{-2}sec^{-1}$) grown WT and *ceh1* seedlings. *DR5-GFP* (green), chloroplast fluorescence (red) and merged images.

284 (ABA) and jasmonic acid (JA) in response to high MEcPP levels in *ceh1* seedlings

(Fig. S5). Similar ABA and JA levels found in WT and *ceh1* plants grown in the dark and in Rc strongly support the specificity of MEcPP-mediated regulation of auxin.

Enhanced tolerance of ceh1 to auxin and auxinole

Reduced IAA levels in *ceh1* led us to examine whether external application of this hormone could rescue the retarded hypocotyl growth in *ceh1* seedlings. The analyses showed longer hypocotyls in *ceh1* seedlings treated with IAA at concentrations (10 and 100 μM) that inhibited growth in WT seedlings (Fig. 5**A**-**B**). Interestingly, *ceh1* and WT hypocotyls displayed similar lengths when treated with the highest IAA concentration used here (100 μM), albeit through two opposing responses, namely growth suppression in WT and induction in *ceh1*.

This finding led to the hypothesis that the enhanced tolerance of *ceh1* to auxin treatment is not solely the result of reduced auxin levels in the mutant, but also a consequence of modified auxin signaling in the mutant. To address this possibility, we treated WT and *ceh1* seedlings with auxinole, an auxin signaling inhibitor that functions as an auxin antagonist for TIR1/AFB receptors (Hayashi et al., 2008; Hayashi et al., 2012). The analyses showed clear dose-dependent suppression of hypocotyl growth of WT seedlings in response to auxinole treatment, in contrast to the unresponsiveness of *ceh1* seedlings at all concentrations examined (Fig. 5**C**-**D**). Collectively, the data indicated enhanced tolerance of *ceh1* to otherwise inhibitory concentrations of auxin and auxinole, likely stemming from reduced auxin levels and compromised signaling in the mutant line.

Altered auxin transport in ceh1

We have previously established that MEcPP-mediated modulation of levels and distribution patterns of auxin (IAA) is via dual transcriptional and post-translational regulatory inputs (Jiang et al., 2018). We specifically demonstrated reduced transcript and protein levels of auxin efflux transporter PIN-FORMED 1 (PIN1) in *ceh1* seedlings grown in white light. Here, we extended these analyses to Rc-grown seedlings, initially by expression analyses of *PIN1* in WT and *ceh1*. The analyses showed similar *PIN1* transcript levels in *ceh1* and the WT seedlings (Fig. 6**A**). By contrast, the combined approaches of immunoblot and immunolocalization analyses

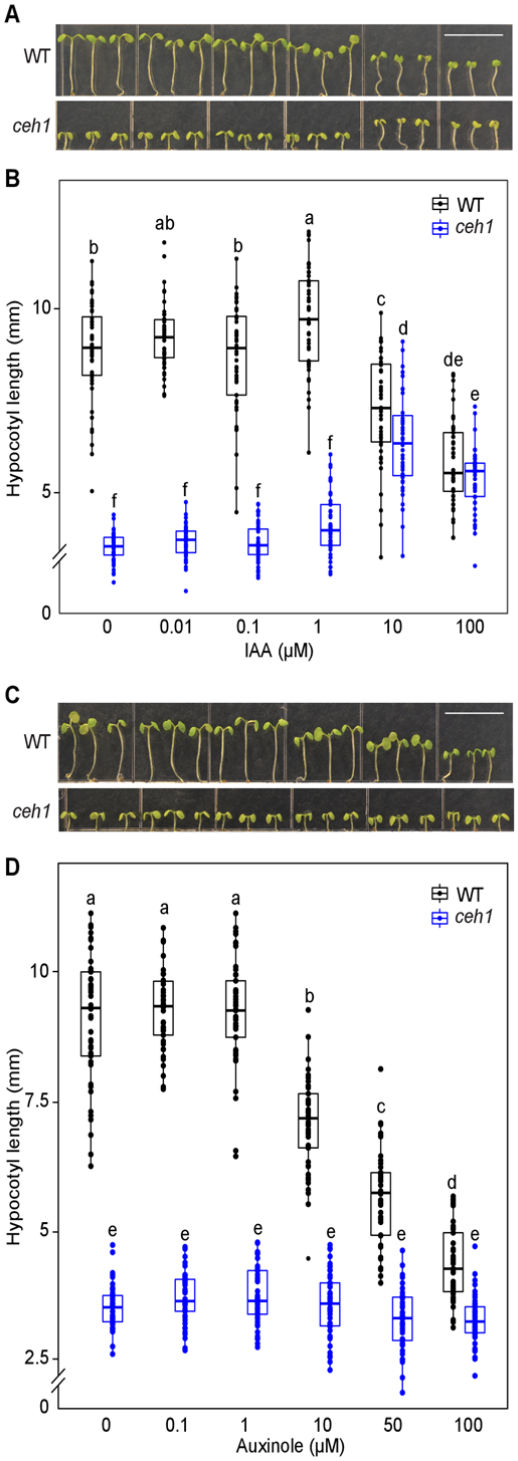

Fig. 5. Enhanced tolerance of *ceh1* to auxin and auxinole
(**A**) & (**C**) Representative images of 7-day-old WT and *ceh1* seedlings in the absence (0) and presence of IAA and auxinole grown under Rc (15 $\mu Em^{-2}sec^{-1}$), respectively. (**B**) & (**D**) Quantification of hypocotyl lengths of seedlings from panel (**A**) & (**C**), respectively. Data are presented with 45 seedlings. The break indicates a change of scale on the y axis. Statistical analyses were carried out using Tukey's HSD method, different letters indicate significant difference ($P < 0.05$). Scale bars: 1cm.

315 confirmed a significant reduction in PIN1 protein levels in *ceh1* compared to WT

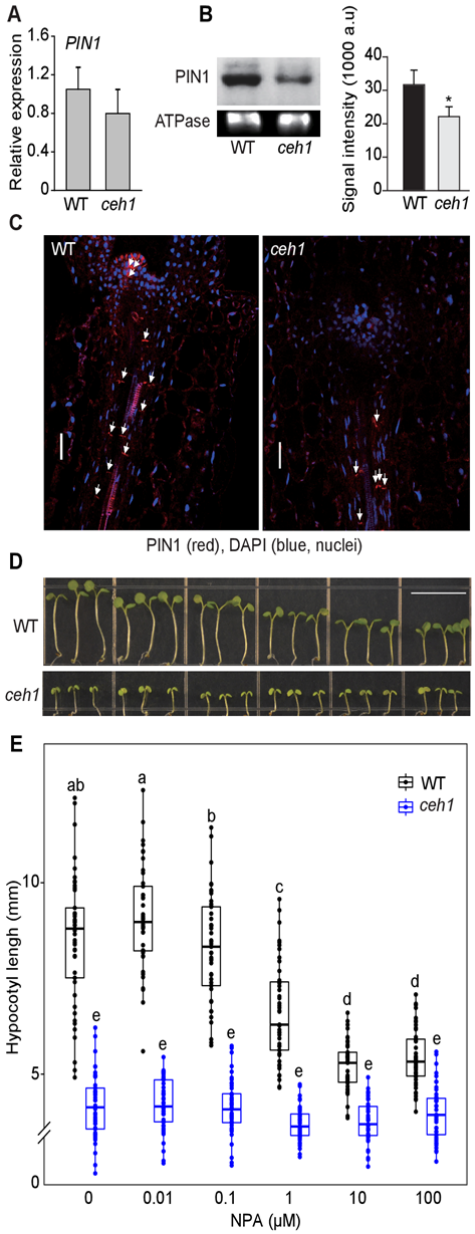

Fig. 6. Altered auxin transport in *ceh1*

(**A**) *PIN1* expression levels in 7-day-old WT and *ceh1* seedlings grown in Rc (15 μEm^{-2}sec^{-1}). Experiment was performed as described in Fig. 4**A**. Data are presented with three biological replicates and three technical replicates.

(**B**) Immunoblots of PIN1 and ATPase as the protein loading control, and signal intensity quantification of the PIN1/ATPase protein abundance in 7-day-old WT and *ceh1* seedlings grown under Rc (15 μEm^{-2}sec^{-1}) with two biological replicates. Asterisk denotes significant difference as determined by a two-tailed Student's *t* tests.

(**C**) Immunolocalization of PIN1 in the hypocotyls of 7-day-old WT and *ceh1* seedlings grown under Rc (15 μEm^{-2}sec^{-1}). Scale bar: 20 μm.

(**D**) Representative images of 7-day-old WT and *ceh1* seedlings grown under Rc (15 μEm^{-2}sec^{-1}) in the absence (0) and presence of NPA. Scale bar: 1cm.

(**E**) Quantification of hypocotyl length of seedlings from panel (**D**). Data are presented with 45 seedlings. Statistical analyses were carried out using Tukey's HSD method. Data are means ± SD and different letters indicate significant difference ($P < 0.05$).

316 seedlings (Fig. 6**B-C**). Specifically, immunolocalization clearly showed reduced PIN1

protein abundance in plasma membranes of xylem parenchyma cells (along tracheids), most notably in the meristems of *ceh1* compared to WT seedlings, albeit with an unchanged polarity (Fig. 6**C**). These data support the earlier finding establishing the role of MEcPP in modulating PIN1 protein abundance both in Rc- and white light–grown seedlings (Jiang et al., 2018).

The reduced levels of the major auxin transporter PIN1 led us to examine the impact of varying concentrations of a general auxin polar transport inhibitor, specifically 1-naphthylphthalamic acid (NPA) (Scanlon, 2003), on the hypocotyl growth of WT and *ceh1* seedlings grown in Rc (Fig. 6**D**-**E**). As expected, NPA application reduced WT hypocotyl growth in a dose-dependent manner, which contrasts the lack of detectable response in *ceh1*, thereby confirming compromised auxin transport in the mutant.

Ethylene regulates hypocotyl growth in ceh1

Comparative transcriptomic profiling of WT and *ceh1* seedlings grown in Rc revealed reduced levels of ethylene biosynthesis genes, *ACSs* (Table S1), in the mutant. This observation, in conjunction with the established crosstalk between ethylene and auxin (Yu et al., 2013; Sun et al., 2015; Das et al., 2016), prompted us to further investigate the potential function of ethylene in regulating *ceh1* hypocotyl growth. Initially, we performed RT-qPCR analyses on ethylene biosynthesis genes to validate the original transcriptomic profile data (Table S1, and Fig. S4). The data showed that compared to WT seedlings, there is a prominent reduction in the transcript levels of *ACS4* in dark- and Rc-grown *ceh1* seedlings (≥2-fold and ~60-fold, respectively), as well as a notable (3–10-fold depending on the gene) reduced expression of *ACS5*, *-6*, and *-8*, albeit solely in Rc-grown *ceh1* (Fig. 7**A**).

Measurements of ethylene in these seedlings confirmed reduced levels (~80%) of the hormone in Rc-grown *ceh1* compared to WT seedlings (Fig. 7**B**). This led us to examine hypocotyl growth of seedlings grown in the presence of varying concentrations of ethylene precursor, ACC (Fig. 7**C**-**D**). The data show suppression of WT hypocotyl growth at all concentrations examined, as opposed to equally enhanced hypocotyl growth in *ceh1* at both ACC concentrations (10 and 20 μM), an indication

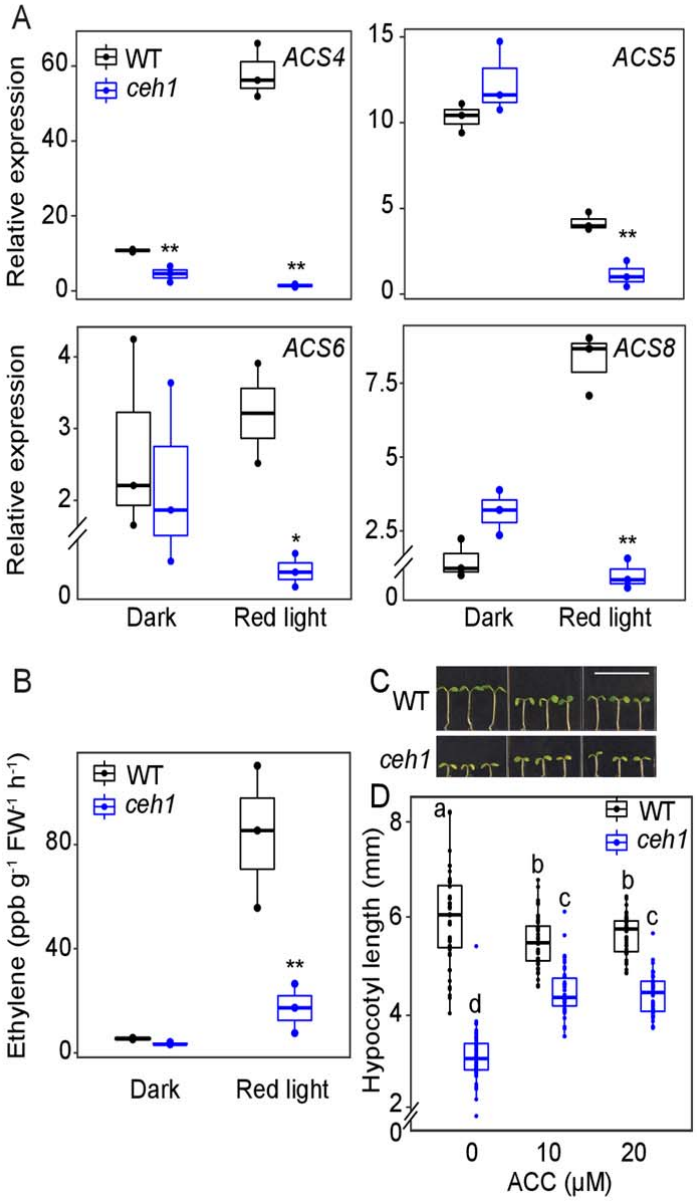

Fig. 7. Ethylene regulates hypocotyl growth in *ceh1*
(**A**) Expression levels of *ACS4*, *5*, *6* and *8* in 7-day-old WT and *ceh1* seedlings grown in the dark and Rc (15 μEm^{-2}sec^{-1}). Experiment was performed as described in Fig. 4**A**. Data are presented with three biological replicates and three technical replicates. Statistical analyses were determined by a two-tailed Student's *t* tests with a significance of $P < 0.05$ *, $P < 0.01$ **. (**B**) Ethylene levels in samples used in panel (**A**). (**C**) Representative images of 7-day-old WT and *ceh1* seedlings grown in the absence (0) and presence of ACC in the Rc (15 μEm^{-2}sec^{-1}). Scale bar: 1cm. (**D**) Quantification of hypocotyl length of seedlings from panel (**C**). Data are presented with 45 seedlings. The break indicates a change of scale on the y axis.Statistical analyses were carried out using Tukey's HSD method, different letters indicate significant difference ($P < 0.05$).

347 of saturation of growth response. Altogether, the data support MEcPP-mediated

coordination of red-light signaling cascades with ethylene levels and ethylene regulation of hypocotyl growth.

Hierarchy of ethylene and auxin signaling pathways

The partial recovery of *ceh1* hypocotyl growth by external application of auxin and ethylene, albeit to varying degrees, prompted us to genetically explore their potential interdependency and hierarchy of their respective growth regulatory actions in Rc-grown seedlings. To address this, we applied ACC and IAA independently to mutant lines *ceh1*; *ceh1* introgressed into auxin receptor mutant *tir1-1* (*ceh1/tir1-1*); and *ceh1* introgressed into single ethylene-signaling mutants *ein3* and *eil1* (*ceh1/ein3*, *ceh1/eil1*) and the double mutant *ein3 eil1* (*ceh1/ein3 eil1*).

Analyses of hypocotyl lengths of Rc-grown WT, *ceh1*, *ceh1/tir1-1*, and *tir1-1* seedlings in the absence and presence of ACC demonstrated TIR1-dependent growth-promoting action of ACC in *tir1-1* and *ceh1/tir1-1* (Fig. 8**A**-**B**). We furthered these studies by applying ACC alone or together with NPA (Fig. 8**C-D**). Consistent with the earlier data, ACC treatment promoted *ceh1* hypocotyl growth, but less effectively when combined with the auxin polar transport inhibitor NPA (Fig. 8**C-D**).

In parallel, we examined hypocotyl growth of Rc-grown WT, *ceh1*, *ein3*, *ceh1/ein3*, *eil1*, *ceh1/eil1*, *ein3/eil1*, and *ceh1*/*ein3eil1* seedlings in the presence and absence of externally applied IAA (Fig. 8**E-F**). Enhanced growth of *ceh1* hypocotyls in the presence of IAA irrespective of mutant backgrounds (single or double *ein3/eil1*) reaffirmed the growth-promoting function of auxin even in lines perturbed in ethylene signaling.

This finding establishes the dependency of ethylene function on auxin signaling, delineating the hierarchy of responses and positioning ethylene as epistatic to the auxin signaling pathway.

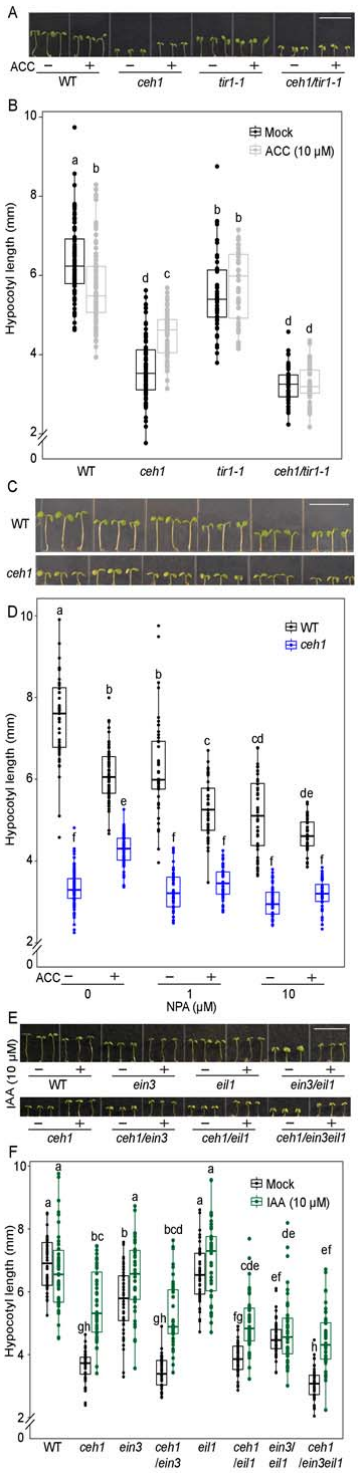

Fig. 8. Ethylene is epistatic to auxin

(**A**) Representative images of 7-day-old WT, *ceh1*, *ceh1/tir1-1* and *tir1-1* seedlings grown in the Rc (15 $\mu Em^{-2}sec^{-1}$) in the absence (-) and presence (+) of ACC. (**C**) Representative images of 7-day-old WT and *ceh1* seedlings grown in the Rc (15 $\mu Em^{-2}sec^{-1}$) in the absence (-) and presence (+) of ACC/NPA alone or in combination. (**E**) Representative images of 7-day-old WT, *ceh1*, *ein3*, *ceh1/ein3*, *eil1*, *ceh1/eil1*, *ein3/eil1*, *ceh1/ein3eil1* seedlings grown in the Rc (15 $\mu Em^{-2}sec^{-1}$) in the absence (-) and presence (+) of IAA.

(**B**) & (**D**) & (**F**) Quantification of hypocotyl length of seedlings from panel (**A**) & (**C**) & (**E**), respectively. Data are presented with 45 seedlings. The break indicates a change of scale on the y axis.Statistical analyses were carried out using Tukey's HSD method, different letters indicate significant difference ($P < 0.05$). Scale bars: 1cm.

Discussion

An inherent feature of plant growth and development is the capacity to coordinate and integrate external cues with endogenous regulatory pathways through tightly regulated signaling cascades. Recent studies have identified retrograde signaling as a quintessential mode of cellular communication required for optimal organismal response to prevailing conditions. Here, we provide a coherent picture of how the stress-specific plastidial retrograde signaling metabolite (MEcPP) coordinates light and hormonal signaling circuitries to adjust growth to the most prevalent environmental cue, light conditions.

Our simplified schematic model (Fig. 9) depicts MEcPP as the upstream signal coordinating and modulating drivers of growth, specifically through enhancing phyB protein abundance and the consequential reduction of auxin levels and distribution in conjunction with diminished ethylene content.

The degradation of phyB is established to be through intermolecular transaction of this photoreceptor with PIF transcription factors (Ni et al., 2013), thereby supporting the prospect of significantly reduced *PIF4* and -5 transcript levels as the likely cause of enhanced phyB protein abundance in *ceh1* seedlings grown in Rc. Furthermore, reversion of *ceh1* stunted hypocotyls in *ceh1/phyB-9* confirms the key role of enhanced phyB protein abundance in growth retardation of the mutant, confirming the earlier finding using white light–grown seedlings (Jiang et al., 2019)

The role of phyB in regulating growth is reported to be through repressing auxin-response genes (Devlin et al., 2003; Halliday et al., 2009). The red light–mediated reduction of auxin biosynthesis and signaling together with decreased hormone levels in *ceh1* supports phyB function in auxin regulation. In addition, reduced levels of PIN1 protein abundance as evidenced by immunoblot and immunolocalization assays suggest the regulatory role of phyB in controlling auxin transport via modulation of PIN1 protein levels. This notion is supported by the ineffectiveness of auxin transport inhibitor in modulating hypocotyl growth of Rc-grown *ceh1* seedlings.

Similar to auxin, reduction of ethylene levels, partly due to decreased transcript levels of the respective biosynthesis genes in Rc-grown *ceh1*, strongly supports the

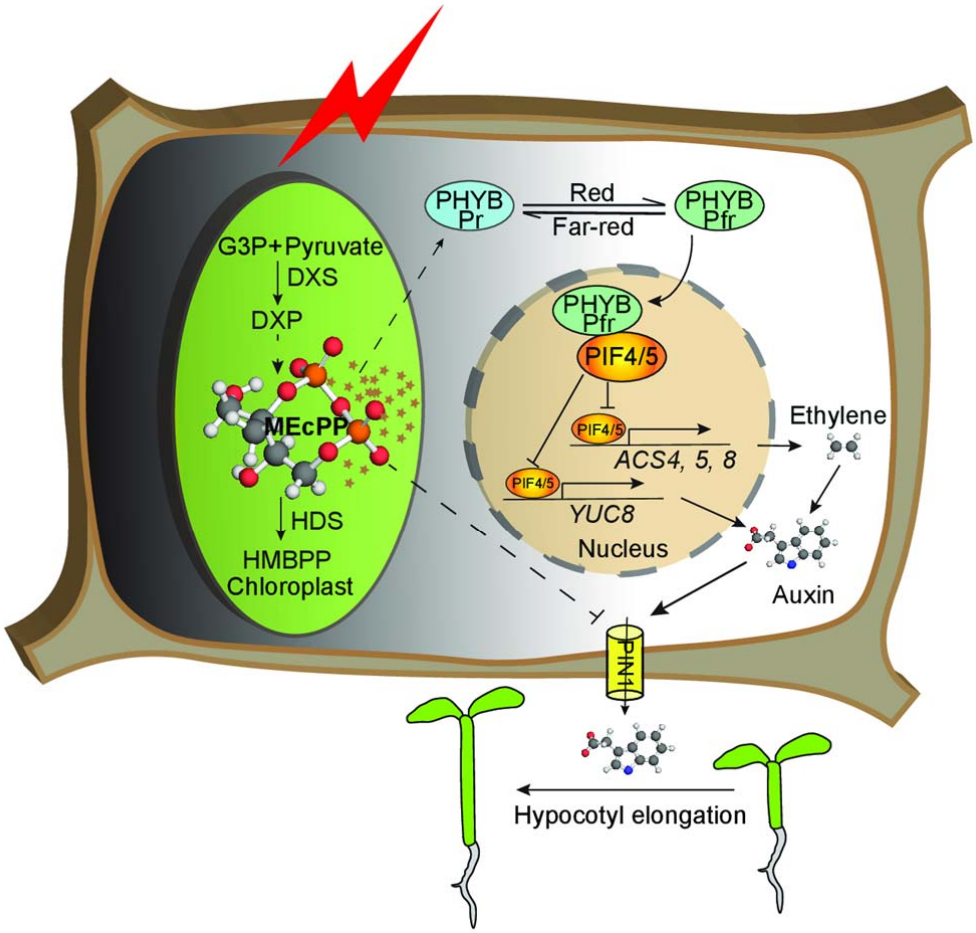

Fig.9. Schematic model depicting MEcPP as the integrator of growth regulating pathways Stress induction of MEcPP accumulation reduces expression of *PIF 4* and *5* and enhances abundance of phyB protein and the consequential orchestration of ethylene-auxin hierarchy to regulate growth.

regulatory role of MEcPP-mediated induction of phyB in the process. Partial and differential recovery of *ceh1* hypocotyl growth under Rc in the presence of external auxin or ACC identifies auxin as the key growth-regulating hormone under these experimental conditions. Moreover, measurement of hypocotyl growth of *ceh1* seedlings introgressed into auxin and ethylene signaling receptor mutants, places ethylene epistatic to auxin, and supports a one-directional control mechanism of ethylene-auxin interaction under Rc conditions.

Conclusions

Here, we revealed MEcPP-mediated enhanced abundance of PhyB, in part via suppression of *PIF4* and -*5* expression levels, and the resulting reduced hypocotyl

growth. We further established MEcPP-mediated coordination of phytochrome B with auxin and ethylene signaling pathways, and the function of the collective signaling circuitries in the regulation of hypocotyl growth of red light–grown seedlings. In addition, hormonal applications and pharmacological treatments support hierarchical functions of auxin and ethylene in regulating growth, with ethylene being epistatic to auxin.

In summary, this finding illustrates MEcPP-mediated coordination of light and hormonal signaling cascades to ultimately reprogram plant growth in responses to the light environment and further provides information on the functional hierarchy of these growth regulatory inputs. As such, this finding identifies plastids as the control hub of growth plasticity in response to environmental cues.

MATERIALS AND METHODS

Plant materials

The wild-type seedlings used here are the earlier-reported Col-0 ecotype transformed with *HPL:LUC* constructs and used as the parent (WT) for isolation of the *ceh1* mutant (Xiao et al., 2012). All experiments were performed with 7-day-old seedlings grown in 15 μE m^{-2} sec^{-1} continuous monochromatic light at 22°C, unless specified otherwise. The *ein3/eil1* double mutant is provided by Hongwei Guo (Southern University of Science and Technology); *DR5*-GFP is a gift from Mark Estelle (University of California, San Diego); and *tir1-1* (CS3798) was ordered from ABRC.

Light treatment

Surface-sterilized seeds were planted on half-strength Murashige and Skoog medium (1/2 MS: 2.2 g/L Murashige and Skoog salts, 1 g/L MES (2-(N-morpholino) ethanesulfonic acid, pH 5.7, and 8 g/L agar), stratified at 4°C for 5 days, grown in 15 μE m^{-2} sec^{-1} of monochromatic red, far-red, and blue LEDs (Quantum Devices Snap-Lite) in a custom chamber at ~ 22°C for 7 days prior to hypocotyl measurement. Dark control experiments were performed by exposing seedlings to white light for 3 hours after stratification, and then wrapping the plates with 3 layers of aluminum foil, and growing seedlings for 7 days before quantification of hypocotyl length. Each treatment was performed on three biological replicates, each replicate with 15

445 seedlings.

446 **Hypocotyl length measurement**

447 Seven-day-old seedlings were scanned with an Epson flatbed scanner, hypocotyl
448 length was measured using Image J.

449 **RNA isolation and RNA-Seq library construction**

450 Total RNA was isolated using TRIzol (Life Technologies) from 7-day-old seedlings
451 grown in the dark and in Rc. The RNA quality and quantity were assessed by
452 Nanodrop ND 1000 (Nanodrop technologies), 4 µg of qualified total RNA was used
453 for RNA-Seq library preparation using Illumina's TruSeq v1 RNA sample Preparation
454 kit (RS-930-2002) with a low-throughput protocol following manufacturer's
455 instructions with modifications as described (Devisetty et al., 2014). Illumina's 12
456 indices were used during adaptor ligation and library construction. The constructed
457 libraries were size-selected using 1:1 volume of AMPure XP beads (Beckman Coulter,
458 Brea CA). Size and quality of libraries were examined using Bioanalyzer 2100
459 (Agilent, Santa Clara, CA). The 12 libraries were quantified using Quant-iT™
460 PicoGreen® ds DNA Assay Kit (Invitrogen) and equally pooled in 1 lane of
461 single-end 50-bp sequencing in HiSeq 2000 machine (Illumina, San Diego, CA) at the
462 QB3 facility at UC Berkeley.

463 **Quality filtering and alignment of RNA-Seq data**

464 To ensure good read quality for downstream analysis, raw reads were pre-processed
465 using FastX-tool kit software (http://hannonlab.cshl.edu/fastx_toolkit/) and custom
466 Perl scripts. First, the de-multiplexed raw reads were filtered with fastq_quality_filter,
467 parameters (−q 20, minimum quality score to keep: 20; −p 95, minimum percent of
468 bases that must satisfy the quality score cut-off: 95). Next, reads with custom adapters
469 were removed using a custom script. Quality of reads was examined before and after
470 quality control with FastQC quality assessment software
471 (http://www.bioinformatics.babraham.ac.uk/projects/fastqc/). Then Reads (1x50 bp)
472 were mapped against the *Arabidopsis* representative_gene_model (TAIR10) using
473 BWA v0.6.1-r104 (Li and Durbin, 2009) with parameters (-l 20) and SAMtools (Li et
474 al., 2009). The resulting BAM files were used to calculate the read counts using a

custom R script, and then the counts were used for differential gene expression analysis.

Differential expression analysis of RNA-Seq data

The EdgeR Bioconductor package implemented in R was used to generate the pseudo-normalized counts for visualization and to carry out differential gene expression analysis (Robinson et al., 2010). Genes were kept for further analysis if read counts were greater than 1 count per million (cpm) in at least 3 of the 12 libraries. The EdgeR Generalized linear models (GLM) framework with explanatory variables of genotype and treatment allowed us to specify a design matrix estimating the effect of run number (batch) as a nuisance parameter. After fitting the model for our experiment, we defined contrasts between parent lines (WT) and mutant (*ceh1*) in red light and tested for significant expression differences using a likelihood ratio test ('glmLRT'). *P*-values for the remaining genes were adjusted using Benjamini-Hochberg method for false discovery correction. Genes with an FDR-adjusted *P*-value less than or equal to 0.01 were identified as differentially expressed.

Multi-dimensional scaling (MDS) plot

A multi-dimensional scaling (MDS) plot was generated in edgeR to analyze relationship between samples. Distance between each pair of RNA-seq profiles corresponded to the average (root-mean-square) of absolute logFC between each pair of samples.

GO Term enrichment

Goseq package in R (Young et al., 2010) was used to identify enriched Gene Ontology (GO) terms (mainly biochemical process) in the differentially expressed gene list.

Hormones and chemical treatments

Surface-sterilized seeds were planted on 1/2 MS, stratified at 4°C for 3 days, germinated under continuous red light at 15 μmol m^{-2} sec^{-1} for 2 days and subsequently transformed to 1/2 MS medium with 1 g/L MES (2-(N-morpholino) ethanesulfonic acid) in combination with hormones or chemicals. These plates were

vertically placed in continuous red light for 5 extra days before hypocotyl measurements. IAA, ACC, auxinole, and NPA were dissolved in ethanol, water, DMSO, and DMSO, respectively. The corresponding solvents were used as control treatment (mock) for the respective experiments.

MEcPP and hormone measurements

Quantification of SA, JA, ABA, and IAA was carried out by gas chromatography-mass spectrometry (GC-MS), using dihydro-JA, deuterated SA, ABA, and IAA as internal standard, respectively, as previously described (Savchenko et al., 2010). MEcPP extraction and quantification was performed as previously described (Jiang et al., 2019).

Microscopy

Confocal fluorescence imaging was performed using Zeiss LSM 710. GFP signal was examined in 7-day-old *DR5*-GFP and *ceh1/DR5*-GFP seedlings grown on 1/2 MS in Rc (15 μE $m^{-2}sec^{-1}$).

Immunolocalization of PIN1

Immunolocalization of PIN1 was performed using anti-PIN1 monoclonal primary antibody and FITC anti mouse secondary antibody as previously described (Jiang et al., 2018).

Reverse Transcription Quantitative PCR

Total RNA was isolated from 7-day-old seedlings grown in the Rc using TRIzol (Life Technologies) and treated with DNase to eliminate DNA contamination. 1 μg total RNA was reverse transcribed into cDNA using SuperScript III (Invitrogen). *At4g26410* was used to normalize target gene expressions. Gene-specific primers were designed using QuantPrime qPCR primer design tool (http://www.quantprime.de/) and are listed (Supplemental Table S2). Each experiment was performed with three biological replicates and three technical replicates.

Protein extraction and immunoblot analyses

For protein extraction 7-day-old seedlings were collected, ground with liquid nitrogen, homogenized in extraction buffer (10 mM Hepes, pH 7.6, 1 M Sucrose, 5 mM KCl, 5 mM $MgCl_2$, 5 mM EDTA, 14 mM 2-ME, 0.4% (W/V) Triton X-100, 0.4 mM PMSF,

20 μM MG132, 20 μM MG115, and Proteinase Inhibitor), centrifuged at $1X10^{-5}G$ for 10 min at 4°C, after which supernatants were transferred to new tubes as total proteins. Then the proteins were separated on 7.5% SDS-PAGE gel and transferred to PVDF membranes. Blots were probed with B1+B7 (1:500) primary antibodies obtained from Peter Quail lab. The secondary was anti-mouse horseradish peroxidase (HRP) (KPL, catalog no. 074-1806) (1:10000). Immunoblots for PIN1 protein were performed as previously described (Jiang et al., 2018) using anti PIN1 monoclonal antibody (1:100) primary antibody and secondary anti-mouse Horseradish peroxidase (HRP) (1:3000). Chemiluminescent reactions were performed using the Pierce ECL Western Blotting Substrate following the manufacturer's instructions. Excess substrate was removed from membranes before placing them between two plastic sheets to develop with X-ray, and subsequently scanned with Epson Perfection V600 Photo Scanner.

Statistical analyses

All experiments were performed with at least three biological replicates. Data are mean ± standard deviation (SD). The statistical analyses were performed using library agricolae, Tukey's HSD test method in R with a significance of $P < 0.05$ (Bunn, 2008). We have specified the method we used for statistical analysis in all figure legends. The names and accession numbers of all genes named in the paper are presented in Table S1.

Accession Numbers

Sequence data from this article can be found in the GenBank/EMBL data libraries under accession numbers **PRJNA601482**.

Supplemental Data

Supplemental Figure S1. Hypocotyl growth of *ceh1* in continuous blue and far-red light is phyB-independent.

Supplemental Figure S2. Expression levels of *PIF1*, *-3*, *-4*, and *-5* in WT and *ceh1* seedlings grown in the dark and Rc (15 $\mu Em^{-2}sec^{-1}$).

Supplemental Figure S3. MDS plot of sequencing data from 7-day-old WT and *ceh1* seedlings grown in the dark and Rc (15 μEm-2sec-1).

Supplemental Figure S4. Heatmap of Top 50 significantly enriched Go terms of down-regulated genes in *ceh1*/WT under continuous Rc (15 µEm-2sec-1).

in *ceh1*/WT under continuous Rc (15 $\mu Em^{-2}sec^{-1}$).

Supplemental Figure S5. Similar ABA and JA levels in WT and *ceh1* seedlings grown in the dark and in Rc (15 $\mu Em^{-2}sec^{-1}$).

Supplemental Table S1. List of differentially expressed genes.

Supplemental Table S2. List of primers used in RT-qPCR analyses.

Acknowledgements

We would like to thank Mr. Derrick R. Hicks (University of Washington) for providing images of ethylene, IAA and MEcPP stick chemical structures depicted in our model. We also would like to thank Prof. Meng Chen and Dr. Yongjian Qiu for providing the red-light chamber and reagents for our experiments, and Dr. Peter Quail for generously providing us with the phyB antibody. We would like to thank Jacob North for all his efforts towards seedling preparation. We are thankful to Dr. Geoffrey Benn for performing the statistical analyses using R program.

Figure legends

Fig. 1. Ceh1 hypocotyl growth in red light is phyB-dependent

(A) Representative images of 7-day-old WT, ceh1, ceh1/phyB-9 and phyB-9 seedlings grown in the dark and continuous red light (Rc: 15 µEm-2sec-1). (**B**) Quantification of hypocotyl lengths from aforementioned genotypes shown in Fig.1A. (**C**) MEcPP levels of samples from Fig.1**A**. The break indicates a change of scale on the y axis. Statistical analyses were performed using Tukey's HSD method ($n \geqslant 45$), different letters indicate significant difference ($P < 0.05$). Scale bars: 1cm.

Fig. 2. MEcPP induction of phyB results in stunted *ceh1* hypocotyl growth

(**A**) Representative images of 7-day-old Col-0, WT, *ceh1* and complementation line (CP) seedlings grown in Rc15 (15 µEm-2sec-1). Scale bars: 1 cm. (**B**) & (**E**) Quantification of hypocotyl length of seedlings from panel (**A**) and (**D**), respectively. Data are presented with 45 seedlings. Statistical analyses were carried out using Tukey's HSD method, different letters indicate significant difference ($P < 0.05$). (**C**) & (**F**) Immunoblots of phyB protein abundance, using RPN6 antibody a loading control. (**D**) Representative images of 7-day-old WT and *ceh1* seedlings grown in Rc15 (15 µEm-2sec-1) in the absence (-) and presence (+) of fosmidomycin (20 µM).

Fig. 3. Overexpression of *PIF4* and *PIF5* recover stunted hypocotyl growth of *ceh1*

(**A**) Quantification of hypocotyl lengths of 7-day-old WT, *ceh1*, *ceh1*/*pifq*, and *pifq* grown in Rc (15 µEm-2sec-1). (**B**) Quantification of hypocotyl lengths from 7-day-old WT, *ceh1*, *ceh1*/*PIF4-OX*, *PIF4-OX*, *ceh1*/*PIF5-OX* and *PIF5-OX* grown in Rc (15 µEm-2sec-1). Data are presented with n≥20 for the *pif* mutant backgrounds and n≥30 for the experiments containing *PIF-OX* seedlings. The break indicates a change of scale on the y axis. Statistical analyses were carried out using Tukey's HSD method, different letters indicate significant difference.

Fig. 4. Auxin is reduced in *ceh1*

Expression levels of *YUC3*, *8* (**A**) and *IAA6*, *19* (**B**) in WT and *ceh1* seedlings. RNAs were extracted from 7-day-old WT and *ceh1*seedlings grown in the dark and Rc (15 µEm-2sec-1). Transcript levels of target genes were normalized to the levels of At4g26410 (M3E9). Data are presented with three biological replicates and three technical replicates. Statistical analyses were determined by a two-tailed Student's *t* tests with a significance of $P < 0.05$ *, $P < 0.01$ **. (**C**) IAA levels in 7-day-old WT and *ceh1* seedlings grown in the dark and Rc (15 µEm-2sec-1). Data are presented with three biological replicates. The break indicates a change of scale on the y axis. Statistical analyses were carried out by a two-tailed Student's *t* tests with a significance of $P < 0.05$. (**D**) Representative images of *DR5-GFP* signal intensity in

7-day hypocotyls of Rc (15 μEm-2sec-1) grown WT and *ceh1* seedlings. *DR5-GFP* (green), chloroplast fluorescence (red) and merged images.

Fig. 5. Enhanced tolerance of *ceh1* to auxin and auxinole

(**A**) & (**C**) Representative images of 7-day-old WT and *ceh1* seedlings in the absence (0) and presence of IAA and auxinole grown under Rc (15 μEm-2sec-1), respectively. (**B**) & (**D**) Quantification of hypocotyl lengths of seedlings from panel (**A**) & (**C**), respectively. Data are presented with 45 seedlings. The break indicates a change of scale on the y axis. Statistical analyses were carried out using Tukey's HSD method, different letters indicate significant difference ($P < 0.05$). Scale bars: 1cm.

Fig. 6. Altered auxin transport in *ceh1*

(**A**) *PIN1* expression levels in 7-day-old WT and *ceh1* seedlings grown in Rc (15 μEm-2sec-1). Experiment was performed as described in Fig. 4**A**. Data are presented with three biological replicates and three technical replicates. (**B**) Immunoblots of PIN1 and ATPase as the protein loading control, and signal intensity quantification of the PIN1/ATPase protein abundance in 7-day-old WT and *ceh1* seedlings grown under Rc (15 μEm-2sec-1) with two biological replicates. Asterisk denotes significant difference as determined by a two-tailed Student's *t* tests. (**C**) Immunolocalization of PIN1 in the hypocotyls of 7-day-old WT and *ceh1* seedlings grown under Rc (15 μEm-2sec-1). Scale bar: 20 μm. (**D**) Representative images of 7-day-old WT and *ceh1* seedlings grown under Rc (15 μEm-2sec-1) in the absence (0) and presence of NPA. Scale bar: 1cm. (**E**) Quantification of hypocotyl length of seedlings from panel (**D**).Data are presented with 45 seedlings. Statistical analyses were carried out using Tukey's HSD method. Data are means ± SD and different letters indicate significant difference ($P < 0.05$).

Fig. 7. Ethylene regulates hypocotyl growth in *ceh1*

(**A**) Expression levels of *ACS4*, *5*, *6* and *8* in 7-day-old WT and *ceh1*seedlings grown in the dark and Rc (15 μEm-2sec-1). Experiment was performed as described in Fig.

4**A**. Data are presented with three biological replicates and three technical replicates. Statistical analyses were determined by a two-tailed Student's *t* tests with a significance of $P < 0.05$ *, $P < 0.01$ **. (**B**) Ethylene levels in samples used in panel (**A**). (**C**) Representative images of 7-day-old WT and *ceh1* seedlings grown in the absence (0) and presence of ACC in the Rc (15 µEm-2sec-1). Scale bar: 1cm. (**D**) Quantification of hypocotyl length of seedlings from panel (**C**). Data are presented with 45 seedlings. The break indicates a change of scale on the y axis. Statistical analyses were carried out using Tukey's HSD method, different letters indicate significant difference ($P < 0.05$).

Fig. 8. Ethylene is epistatic to auxin

(**A**) Representative images of 7-day-old WT, *ceh1*, *ceh1*/*tir1-1* and *tir1-1* seedlings grown in the Rc (15 µEm-2sec-1) in the absence (-) and presence (+) of ACC. (**C**) Representative images of 7-day-old WT and *ceh1* seedlings grown in the Rc (15 µEm-2sec-1) in the absence (-) and presence (+) of ACC/NPA alone or in combination. (**E**) Representative images of 7-day-old WT, *ceh1*, *ein3*, *ceh1*/*ein3*, *eil1*, *ceh1*/*eil1*, *ein3/eil1*, *ceh1*/*ein3eil1* seedlings grown in the Rc (15 µEm-2sec-1) in the absence (-) and presence (+) of IAA. (**B**) & (**D**) & (**F**) Quantification of hypocotyl length of seedlings from panel (**A**) & (**C**) & (**E**), respectively. Data are presented with 45 seedlings. The break indicates a change of scale on the y axis. Statistical analyses were carried out using Tukey's HSD method, different letters indicate significant difference ($P < 0.05$). Scale bars: 1cm.

Fig.9. Schematic model depicting MEcPP as the integrator of growth regulating pathways. Stress induction of MEcPP accumulation reduces expression of *PIF 4* and *5* and enhances abundance of phyB protein and the consequential orchestration of ethylene-auxin hierarchy to regulate growth.

686

Parsed Citations

Bjornson, M., Balcke, G.U., Xiao, Y., de Souza, A., Wang, J.Z., Zhabinskaya, D., Tagkopoulos, I., Tissier, A., and Dehesh, K. (2017). Integrated omics analyses of retrograde signaling mutant delineate interrelated stress-response strata. Plant J 91, 70-84.
Pubmed: Author and Title
Google Scholar: Author Only Title Only Author and Title

Bunn, A.G. (2008). A dendrochronology program library in R (dplR). Dendrochronologia 26, 115-124.
Pubmed: Author and Title
Google Scholar: Author Only Title Only Author and Title

Chai, T., Zhou, J., Liu, J., and Xing, D. (2015). LSD1 and HY5 antagonistically regulate red light induced-programmed cell death in Arabidopsis. Front Plant Sci 6, 292.
Pubmed: Author and Title
Google Scholar: Author Only Title Only Author and Title

Chenge-Espinosa, M., Cordoba, E., Romero-Guido, C., Toledo-Ortiz, G., and Leon, P. (2018). Shedding light on the methylerythritol phosphate (MEP)-pathway: long hypocotyl 5 (HY5)/phytochrome-interacting factors (PIFs) transcription factors modulating key limiting steps. Plant J 96, 828-841.
Pubmed: Author and Title
Google Scholar: Author Only Title Only Author and Title

Das, D., St Onge, K.R., Voesenek, L.A., Pierik, R., and Sasidharan, R. (2016). Ethylene- and shade-induced hypocotyl elongation share transcriptome patterns and functional regulators. Plant Physiol.
Pubmed: Author and Title
Google Scholar: Author Only Title Only Author and Title

De Grauwe, L., Vandenbussche, F., Tietz, O., Palme, K., and Van Der Straeten, D. (2005). Auxin, ethylene and brassinosteroids: tripartite control of growth in the Arabidopsis hypocotyl. Plant & cell physiology 46, 827-836.
Pubmed: Author and Title
Google Scholar: Author Only Title Only Author and Title

de Wit, M., Lorrain, S., and Fankhauser, C. (2014). Auxin-mediated plant architectural changes in response to shade and high temperature. Physiologia plantarum 151, 13-24.
Pubmed: Author and Title
Google Scholar: Author Only Title Only Author and Title

Devisetty, U.K., Covington, M.F., Tat, A.V., Lekkala, S., and Maloof, J.N. (2014). Polymorphism identification and improved genome annotation of Brassica rapa through Deep RNA sequencing. G3 (Bethesda) 4, 2065-2078.
Pubmed: Author and Title
Google Scholar: Author Only Title Only Author and Title

Devlin, P.F., Yanovsky, M.J., and Kay, S.A. (2003). A genomic analysis of the shade avoidance response in Arabidopsis. Plant physiology 133, 1617-1629.
Pubmed: Author and Title
Google Scholar: Author Only Title Only Author and Title

Franklin, K.A., Lee, S.H., Patel, D., Kumar, S.V., Spartz, A.K., Gu, C., Ye, S., Yu, P., Breen, G., Cohen, J.D., Wigge, P.A., and Gray, W.M. (2011). Phytochrome-interacting factor 4 (PIF4) regulates auxin biosynthesis at high temperature. Proceedings of the National Academy of Sciences of the United States of America 108, 20231-20235.
Pubmed: Author and Title
Google Scholar: Author Only Title Only Author and Title

Galweiler, L., Guan, C., Muller, A., Wisman, E., Mendgen, K., Yephremov, A., and Palme, K. (1998). Regulation of polar auxin transport by AtPIN1 in Arabidopsis vascular tissue. Science 282, 2226-2230.
Pubmed: Author and Title
Google Scholar: Author Only Title Only Author and Title

Geldner, N., Friml, J., Stierhof, Y.D., Jurgens, G., and Palme, K. (2001). Auxin transport inhibitors block PIN1 cycling and vesicle trafficking. Nature 413, 425-428.
Pubmed: Author and Title
Google Scholar: Author Only Title Only Author and Title

Gonzalez-Cabanelas, D., Wright, L.P., Paetz, C., Onkokesung, N., Gershenzon, J., Rodriguez-Concepcion, M., and Phillips, M.A. (2015). The diversion of 2-C-methyl-D-erythritol-2,4-cyclodiphosphate from the 2-C-methyl-D-erythritol 4-phosphate pathway to hemiterpene glycosides mediates stress responses in Arabidopsis thaliana. The Plant journal : for cell and molecular biology 82, 122-137.
Pubmed: Author and Title
Google Scholar: Author Only Title Only Author and Title

Halliday, K.J., Martinez-Garcia, J.F., and Josse, E.M. (2009). Integration of light and auxin signaling. Cold Spring Harbor perspectives in biology 1, a001586.
Pubmed: Author and Title
Google Scholar: Author Only Title Only Author and Title

Hayashi, K., Tan, X., Zheng, N., Hatate, T., Kimura, Y., Kepinski, S., and Nozaki, H. (2008). Small-molecule agonists and antagonists of F-box protein-substrate interactions in auxin perception and signaling. Proceedings of the National Academy of Sciences of the United States of America 105, 5632-5637.
Pubmed: Author and Title
Google Scholar: Author Only Title Only Author and Title

Hayashi, K., Neve, J., Hirose, M., Kuboki, A., Shimada, Y., Kepinski, S., and Nozaki, H. (2012). Rational design of an auxin antagonist of the SCF(TIR1) auxin receptor complex. ACS Chem Biol 7, 590-598.
Pubmed: Author and Title
Google Scholar: Author Only Title Only Author and Title

Hornitschek, P., Kohnen, M.V., Lorrain, S., Rougemont, J., Ljung, K., Lopez-Vidriero, I., Franco-Zorrilla, J.M., Solano, R., Trevisan, M., Pradervand, S., Xenarios, I., and Fankhauser, C. (2012a). Phytochrome interacting factors 4 and 5 control seedling growth in changing light conditions by directly controlling auxin signaling. Plant J 71, 699-711.
Pubmed: Author and Title
Google Scholar: Author Only Title Only Author and Title

Hornitschek, P., Kohnen, M.V., Lorrain, S., Rougemont, J., Ljung, K., Lopez-Vidriero, I., Franco-Zorrilla, J.M., Solano, R., Trevisan, M., Pradervand, S., Xenarios, I., and Fankhauser, C. (2012b). Phytochrome interacting factors 4 and 5 control seedling growth in changing light conditions by directly controlling auxin signaling. The Plant journal : for cell and molecular biology 71, 699-711.
Pubmed: Author and Title
Google Scholar: Author Only Title Only Author and Title

J. Jensen, P., P. Hangarter, R., and Estelle, M. (1998). Auxin Transport Is Required for Hypocotyl Elongation in Light-Grown but Not Dark-Grown Arabidopsis. plant Physiol 116, 455-462.
Pubmed: Author and Title
Google Scholar: Author Only Title Only Author and Title

Jiang, J., Zeng, L., Ke, H., De La Cruz, B., and Dehesh, K. (2019). Orthogonal regulation of phytochrome B abundance by stress-specific plastidial retrograde signaling metabolite. Nature communications 10, 2904.
Pubmed: Author and Title
Google Scholar: Author Only Title Only Author and Title

Jiang, J., Rodriguez-Furlan, C., Wang, J.Z., de Souza, A., Ke, H., Pasternak, T., Lasok, H., Ditengou, F.A., Palme, K., and Dehesh, K. (2018). Interplay of the two ancient metabolites auxin and MEcPP regulates adaptive growth. Nature communications 9, 2262.
Pubmed: Author and Title
Google Scholar: Author Only Title Only Author and Title

L.-C. Wang, K., Li, H., and R.Ecker, J. (2002). Ethylene Biosynthesis and Signaling Networks. The plant cell, 131-151.
Pubmed: Author and Title
Google Scholar: Author Only Title Only Author and Title

Leivar, P., and Quail, P.H. (2011). PIFs: pivotal components in a cellular signaling hub. Trends in plant science 16, 19-28.
Pubmed: Author and Title
Google Scholar: Author Only Title Only Author and Title

Leivar, P., and Monte, E. (2014). PIFs: Systems Integrators in Plant Development. Plant Cell 26, 56-78.
Pubmed: Author and Title
Google Scholar: Author Only Title Only Author and Title

Leivar, P., Monte, E., Cohn, M.M., and Quail, P.H. (2012). Phytochrome signaling in green Arabidopsis seedlings: impact assessment of a mutually negative phyB-PIF feedback loop. Molecular plant 5, 734-749.
Pubmed: Author and Title
Google Scholar: Author Only Title Only Author and Title

Lemos, M., Xiao, Y., Bjornson, M., Wang, J.Z., Hicks, D., Souza, A., Wang, C.Q., Yang, P., Ma, S., Dinesh-Kumar, S., and Dehesh, K. (2016). The plastidial retrograde signal methyl erythritol cyclopyrophosphate is a regulator of salicylic acid and jasmonic acid crosstalk. J Exp Bot 67, 1557-1566.
Pubmed: Author and Title
Google Scholar: Author Only Title Only Author and Title

Li, H., and Durbin, R. (2009). Fast and accurate short read alignment with Burrows-Wheeler transform. Bioinformatics 25, 1754-1760.
Pubmed: Author and Title
Google Scholar: Author Only Title Only Author and Title

Li, H., Handsaker, B., Wysoker, A., Fennell, T., Ruan, J., Homer, N., Marth, G., Abecasis, G., Durbin, R., and Genome Project Data Processing, S. (2009). The Sequence Alignment/Map format and SAMtools. Bioinformatics 25, 2078-2079.
Pubmed: Author and Title
Google Scholar: Author Only Title Only Author and Title

Liang, X., Wang, H., Mao, L., Hu, Y., Dong, T., Zhang, Y., Wang, X., and Bi, Y. (2012). Involvement of COP1 in ethylene- and light-regulated hypocotyl elongation. Planta 236, 1791-1802.
Pubmed: Author and Title
Google Scholar: Author Only Title Only Author and Title

Morelli, G., and Ruberti, I. (2002). Light and shade in the photocontrol of Arabidopsis growth. Trends in plant science 7, 399-404.
Pubmed: Author and Title
Google Scholar: Author Only Title Only Author and Title

Nagy, F., and Schafer, E. (2002). Phytochromes control photomorphogenesis by differentially regulated, interacting signaling pathways in higher plants. Annual review of plant biology 53, 329-355.
Pubmed: Author and Title
Google Scholar: Author Only Title Only Author and Title

Negi, S., Sukumar, P., Liu, X., Cohen, J.D., and Muday, G.K. (2010). Genetic dissection of the role of ethylene in regulating auxin-dependent lateral and adventitious root formation in tomato. Plant J 61, 3-15.
Pubmed: Author and Title
Google Scholar: Author Only Title Only Author and Title

Ni, W., Xu, S.L., Chalkley, R.J., Pham, T.N., Guan, S., Maltby, D.A., Burlingame, A.L., Wang, Z.Y., and Quail, P.H. (2013). Multisite light-induced phosphorylation of the transcription factor PIF3 is necessary for both its rapid degradation and concomitant negative feedback modulation of photoreceptor phyB levels in Arabidopsis. The Plant cell 25, 2679-2698.
Pubmed: Author and Title
Google Scholar: Author Only Title Only Author and Title

Nozue, K., Harmer, S.L., and Maloof, J.N. (2011). Genomic Analysis of Circadian Clock-, Light-, and Growth-Correlated Genes Reveals PHYTOCHROME-INTERACTING FACTOR5 as a Modulator of Auxin Signaling in Arabidopsis. Plant Physiol 156, 357-372.
Pubmed: Author and Title
Google Scholar: Author Only Title Only Author and Title

Nozue, K., Devisetty, U.K., Lekkala, S., Mueller-Moule, P., Bak, A., Casteel, C.L., and Maloof, J.N. (2018). Network Analysis Reveals a Role for Salicylic Acid Pathway Components in Shade Avoidance. Plant Physiol 178, 1720-1732.
Pubmed: Author and Title
Google Scholar: Author Only Title Only Author and Title

Pedmale, U.V., Huang, S.C., Zander, M., Cole, B.J., Hetzel, J., Ljung, K., Reis, P.A.B., Sridevi, P., Nito, K., Nery, J.R., Ecker, J.R., and Chory, J. (2016). Cryptochromes Interact Directly with PIFs to Control Plant Growth in Limiting Blue Light. Cell 164, 233-245.
Pubmed: Author and Title
Google Scholar: Author Only Title Only Author and Title

Quail, P.H. (2002). Photosensory perception and signalling in plant cells: new paradigms? Current opinion in cell biology 14, 180-188.
Pubmed: Author and Title
Google Scholar: Author Only Title Only Author and Title

Rausenberger, J., Hussong, A., Kircher, S., Kirchenbauer, D., Timmer, J., Nagy, F., Schafer, E., and Fleck, C. (2010). An Integrative Model for Phytochrome B Mediated Photomorphogenesis: From Protein Dynamics to Physiology. Plos One 5.
Pubmed: Author and Title
Google Scholar: Author Only Title Only Author and Title

Robinson, M.D., McCarthy, D.J., and Smyth, G.K. (2010). edgeR: a Bioconductor package for differential expression analysis of digital gene expression data. Bioinformatics 26, 139-140.
Pubmed: Author and Title
Google Scholar: Author Only Title Only Author and Title

Ruzicka, K., Ljung, K., Vanneste, S., Podhorska, R., Beeckman, T., Friml, J., and Benkova, E. (2007). Ethylene regulates root growth through effects on auxin biosynthesis and transport-dependent auxin distribution. The Plant cell 19, 2197-2212.
Pubmed: Author and Title
Google Scholar: Author Only Title Only Author and Title

Savchenko, T., Walley, J.W., Chehab, E.W., Xiao, Y., Kaspi, R., Pye, M.F., Mohamed, M.E., Lazarus, C.M., Bostock, R.M., and Dehesh, K. (2010). Arachidonic acid: an evolutionarily conserved signaling molecule modulates plant stress signaling networks. The Plant cell 22, 3193-3205.
Pubmed: Author and Title
Google Scholar: Author Only Title Only Author and Title

Scanlon, M.J. (2003). The polar auxin transport inhibitor N-1-naphthylphthalamic acid disrupts leaf initiation, KNOX protein regulation, and formation of leaf margins in maize. Plant Physiol 133, 597-605.
Pubmed: Author and Title
Google Scholar: Author Only Title Only Author and Title

Sellaro, R., Pacin, M., and Casal, J.J. (2012). Diurnal dependence of growth responses to shade in Arabidopsis: role of hormone, clock, and light signaling. Molecular plant 5, 619-628.
Pubmed: Author and Title
Google Scholar: Author Only Title Only Author and Title

Smalle, J., Haegman, M., Kurepa, J., Van Montagu, M., and Van Der Straeten, D. (1997). Ethylene can stimulate Arabidopsis hypocotyl elongation in the light. P Natl Acad Sci USA 94, 2756-2761.
Pubmed: Author and Title
Google Scholar: Author Only Title Only Author and Title

Stepanova, A.N., Yun, J., Likhacheva, A.V., and Alonso, J.M. (2007). Multilevel interactions between ethylene and auxin in Arabidopsis roots. Plant Cell 19, 2169-2185.
Pubmed: Author and Title
Google Scholar: Author Only Title Only Author and Title

Sun, J., Ma, Q., and Mao, T. (2015). Ethylene Regulates the Arabidopsis Microtubule-Associated Protein WAVE-DAMPENED2-LIKE5 in Etiolated Hypocotyl Elongation. Plant Physiol 169, 325-337.
Pubmed: Author and Title
Google Scholar: Author Only Title Only Author and Title

Swarup, R., Perry, P., Hagenbeek, D., Van Der Straeten, D., Beemster, G.T.S., Sandberg, G., Bhalerao, R., Ljung, K., and Bennett, M.J. (2007). Ethylene upregulates auxin biosynthesis in Arabidopsis seedlings to enhance inhibition of root cell elongation. Plant Cell 19, 2186-2196.
Pubmed: Author and Title
Google Scholar: Author Only Title Only Author and Title

Tanaka, S., Nakamura, S., Mochizuki, N., and Nagatani, A. (2002a). Phytochrome in cotyledons regulates the expression of genes in the hypocotyl through auxin-dependent and -independent pathways. Plant & cell physiology 43, 1171-1181.
Pubmed: Author and Title
Google Scholar: Author Only Title Only Author and Title

Tanaka, S.I., Nakamura, S., Mochizuki, N., and Nagatani, A. (2002b). Phytochrome in cotyledons regulates the expression of genes in the hypocotyl through auxin-dependent and -independent pathways. Plant and Cell Physiology 43, 1171-1181.
Pubmed: Author and Title
Google Scholar: Author Only Title Only Author and Title

Tian, Q., Uhlir, N.J., and Reed, J.W. (2002). Arabidopsis SHY2/IAA3 inhibits auxin-regulated gene expression. The Plant cell 14, 301-319.
Pubmed: Author and Title
Google Scholar: Author Only Title Only Author and Title

Vandenbussche, F., Vaseva, I., Vissenberg, K., and Van Der Straeten, D. (2012). Ethylene in vegetative development: a tale with a riddle. The New phytologist 194, 895-909.
Pubmed: Author and Title
Google Scholar: Author Only Title Only Author and Title

Vandenbussche, F., Smalle, J., Le, J., Saibo, N.J., De Paepe, A., Chaerle, L., Tietz, O., Smets, R., Laarhoven, L.J., Harren, F.J., Van Onckelen, H., Palme, K., Verbelen, J.P., and Van Der Straeten, D. (2003). The Arabidopsis mutant alh1 illustrates a cross talk between ethylene and auxin. Plant Physiol 131, 1228-1238.
Pubmed: Author and Title
Google Scholar: Author Only Title Only Author and Title

Walley, J., Xiao, Y., Wang, J.Z., Baidoo, E.E., Keasling, J.D., Shen, Z., Briggs, S.P., and Dehesh, K. (2015). Plastid-produced interorgannellar stress signal MEcPP potentiates induction of the unfolded protein response in endoplasmic reticulum. Proceedings of the National Academy of Sciences of the United States of America 112, 6212-6217.
Pubmed: Author and Title
Google Scholar: Author Only Title Only Author and Title

Wang, J.Z., Li, B., Xiao, Y., Ni, Y., Ke, H., Yang, P., de Souza, A., Bjornson, M., He, X., Shen, Z., Balcke, G.U., Briggs, S.P., Tissier, A., Kliebenstein, D.J., and Dehesh, K. (2017a). Initiation of ER Body Formation and Indole Glucosinolate Metabolism by the Plastidial Retrograde Signaling Metabolite, MEcPP. Molecular plant 10, 1400-1416.
Pubmed: Author and Title
Google Scholar: Author Only Title Only Author and Title

Wang, J.Z., Li, B.H., Xiao, Y.M., Ni, Y., Ke, H.Y., Yang, P.Y., de Souza, A., Bjornson, M., He, X., Shen, Z.X., Balcke, G.U., Briggs, S.P., Tissier, A., Kliebenstein, D.J., and Dehesh, K. (2017b). Initiation of ER Body Formation and Indole Glucosinolate Metabolism by the Plastidial Retrograde Signaling Metabolite, MEcPP. Molecular plant 10, 1400-1416.
Pubmed: Author and Title
Google Scholar: Author Only Title Only Author and Title

Xiao, Y., Savchenko, T., Baidoo, E.E., Chehab, W.E., Hayden, D.M., Tolstikov, V., Corwin, J.A., Kliebenstein, D.J., Keasling, J.D., and Dehesh, K. (2012). Retrograde signaling by the plastidial metabolite MEcPP regulates expression of nuclear stress-response genes. Cell 149, 1525-1535.
Pubmed: Author and Title
Google Scholar: Author Only Title Only Author and Title

Yang, S.F., and Hoffman, N.E. (1984). Ethylene Biosynthesis and Its Regulation in Higher-Plants. Annu Rev Plant Phys 35, 155-189.
Pubmed: Author and Title
Google Scholar: Author Only Title Only Author and Title

Young, M.D., Wakefield, M.J., Smyth, G.K., and Oshlack, A. (2010). Gene ontology analysis for RNA-seq: accounting for selection bias. Genome Biol 11, R14.
Pubmed: Author and Title
Google Scholar: Author Only Title Only Author and Title

Yu, X., Liu, H., Klejnot, J., and Lin, C. (2010). The Cryptochrome Blue Light Receptors. The arabidopsis book 8, e0135.
Pubmed: Author and Title
Google Scholar: Author Only Title Only Author and Title

Yu, Y., Wang, J., Zhang, Z., Quan, R., Zhang, H., Deng, X.W., Ma, L., and Huang, R. (2013). Ethylene promotes hypocotyl growth and HY5 degradation by enhancing the movement of COP1 to the nucleus in the light. PLoS genetics 9, e1004025.
Pubmed: Author and Title
Google Scholar: Author Only Title Only Author and Title

Zhao, Y. (2012). Auxin biosynthesis: a simple two-step pathway converts tryptophan to indole-3-acetic acid in plants. Mol Plant 5, 334-338.
Pubmed: Author and Title
Google Scholar: Author Only Title Only Author and Title

Zhong, S., Shi, H., Xue, C., Wang, L., Xi, Y., Li, J., Quail, P.H., Deng, X.W., and Guo, H. (2012). A molecular framework of light-controlled phytohormone action in Arabidopsis. Curr Biol 22, 1530-1535.
Pubmed: Author and Title
Google Scholar: Author Only Title Only Author and Title